Vrije Universiteit Brussel

![VUB Vrije Universiteit Brussel logo]

On the use of acoustic emission to identify the dominant stress/strain component in carbon/epoxy composite materials

Kalteremidou, Kalliopi-Artemi; Angelis, Dimitrios; Van Hemelrijck, Danny; Pyl, Lincy

On the use of acoustic emission to identify the dominant stress/strain component in carbon/epoxy composite materials

Kalliopi-Artemi KALTEREMIDOU[1*], Dimitrios G. AGGELIS[1], Danny VAN HEMELRIJCK[1], Lincy PYL[1]

[1]*Vrije Universiteit Brussel, Pleinlaan 2, 1050 Brussels, Belgium*
*Corresponding author Kalliopi-Artemi.Kalteremidou@vub.be
 Tel.:+32-26-29-2924
 Accepted:

Abstract

Acoustic Emission (AE) is casually employed for monitoring the mechanical behaviour of composite media as the amount of damage and the different fracture modes can be well characterised through the evolution of the AE characteristics. However, the sensitivity of the technique allows for more than just classification of the existing damage modes in composite materials. In the present paper, the limits of AE are further pushed as it is used to characterise the stress/strain field developing in composite laminates even before damage mechanisms become evident. In addition, the change of the strain field due to damage evolution during quasi-static and fatigue experiments, as monitored by real-time Digital Image Correlation (DIC), is depicted on the shift of the AE parameters. This is of great importance in cases that detrimental shear stresses are generated in the material, leading to important interlaminar delaminations and mechanical deterioration. AE can be used in this direction to predict the upcoming damage modes and to take the necessary measures to avoid final catastrophic failure by applying intermediate repair approaches. The examined material in this study is angle-ply Carbon Fibre Reinforced Polymer (CFRP) composite laminates consisting of different off-axis plies, in which different multiaxial conditions are generated due to the inherent anisotropy of composite materials. It is demonstrated that AE can identify the dominant stress/strain component rather than just the occurring damage mode even at early loading stages, before severe fracture influences the mechanical capacity of the material.

1. Introduction

Acoustic Emission (AE) is a non-destructive method [1] which has been widely used for damage studies in composites [2-5]. In practice, piezoelectric sensors are mounted on the surface and record the elastic waves generated in a material undergoing irreversible changes. The wave magnitude and further features are correlated to emission sources. Firstly, the total AE activity can be examined, giving information on the "amount" of developing damage [6-8]. Secondly, analysis of waveform features in the time domain can be used as damage indicator [9-12]. In other studies, waveform analysis in the frequency domain is performed and clustering approaches for identification of certain damage modes have been many times reported [13-18]. However, to the authors' best knowledge, no direct correlation of AE features with the stress/strain states in polymer composites has been performed in literature.

At the same time, due to the intrinsic anisotropy of composites, multiaxial stresses occur even in flat laminates under simple tensile loads, because of the different fibre orientations in their individual layers [18-21]. However, the AE response of composites has been mostly investigated for individual cases of conventional lay-ups (i.e. [0º/90º], [±45º]) [2-17] or for representative test specimens with specified model damage sources (double cantilever beam specimens [22] or single fibre filaments [23]). Certain correlations between AE parameters and specific fracture modes have been established, like delaminations resulting in longer duration and lower frequencies than matrix cracks or fibre rupture [24-26]. Despite the fact that multiaxial stress conditions occur in all composite structures in the microscale due to their anisotropic nature, in conventional lay-ups the dominant stress state remains largely uniaxial in the lamina level. Thus, it would be of great interest to study the potential

of AE to indicate the dominant stress/strain component rather than just the occurring damage mode when the stress state is multiaxial and especially during the very early loading stages.

Taking the above into account, a thorough experimental campaign was performed in this study to obtain a successive AE analysis of carbon/epoxy laminates, in which different multiaxial stresses are developed. Two laminates, namely $[0^o/30^o]_{2s}$ and $[0^o/60^o]_{2s}$, were thus tested under quasi-static, fatigue and incremental tensile loading. Due to the different fibre orientations, shear stresses govern the stress state in the 30° plies, while normal transverse stresses are the dominant ones in the 60° plies [27]. It is shown through this study that certain AE features can be used to identify the dominant stress/strain component at the early loading stages, before the occurrence of severe damage. At a later stage, damage modes can be also identified through AE feature analysis. One of the most beneficial aspects of the employed methodology is that the AE findings are correlated to real-time fracture scans and not to just theoretical damage modes, useful throughout the whole loading, being sensitive to the developed strain field at low loads, as well as to damage modes as the load increases.

2. Methodology and experimental details

2.1. Material and reasoning of lay-up selection

The material used for this study was a pre-preg carbon fibre/epoxy matrix composite, manufactured by Mitsubishi Chemical Corporation and Honda R&D Co., Ltd., and cured in a flat plate geometry by using compression moulding at a temperature of 140 ℃ and a pressure of 8 MPa. The plates were tabbed on both sides by using the material in a $[\pm45^o]_{2s}$ lay-up to guarantee failure far away from the grips. Samples were cut following ASTM D3039 [28] and had a length of 250 mm, a width of 25 mm and a thickness of 1.83 mm.
Two angle-ply unbalanced laminates, $[0^o/30^o]_{2s}$ and $[0^o/60^o]_{2s}$, were tested during this research work. The lay-ups were selected in such a way that different multiaxial stresses are developed in their off-axis layers. In order to express the different multiaxiality, the biaxiality ratios λ can be used, which indicate the relation between the σ_1, σ_2 and σ_6 stress components in the material coordinate system and are defined as shown in **Fig. 1** [20]. By using the classical laminate theory, the λ ratios can be calculated. As shown in **Fig. 1**, the λ_{12} ratio is equal to 2.02 in the off-axis layers of the $[0^o/30^o]_{2s}$ laminates and equal to 0.64 in the $[0^o/60^o]_{2s}$ laminates. This shows that the shear stress component σ_6 is the dominant one in the off-axis layers of the $[0^o/30^o]_{2s}$ laminates whereas the transverse stress σ_2 dominates in the $[0^o/60^o]_{2s}$ laminates. Taking into account the λ_1 and λ_2 ratios, it can be concluded that σ_1 is in the same order of magnitude as σ_2 and σ_6 in the off-axis plies for both laminates. This shows that the damage in the off-axis layers of the angle-ply laminates is matrix related, affected by the dominant σ_2 or σ_6 stresses. Therefore, a direct comparison between the two lay-ups can be done. The presence of the 0° layers is nevertheless of high importance, in order to guarantee that damage initiates and propagates avoiding brittle failure, as it would be the case if only off-axis layers were inserted in the laminates.
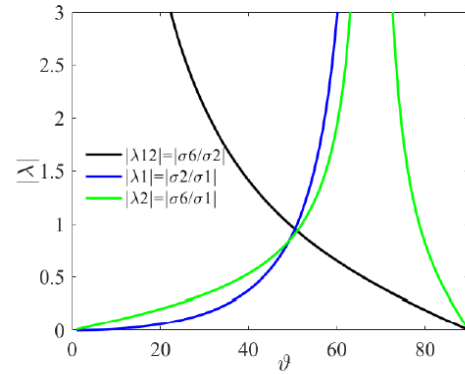

Fig. 1. Evolution of biaxiality ratios as a function of the angle θ of a $[0^o/\theta]_{2s}$ carbon/epoxy laminate.

In order to highlight the AE findings related to the identification of multiaxiality in the angle-ply laminates, the results are also compared with those from more conventional $[0^o/90^o]_{2s}$ and $[\pm45^o]_{2s}$ laminates from the same material.

2.2. Experimental methodology

- An MTS servo-hydraulic test bench with a load capacity of 100 kN was used to perform the tensile tests. Initially quasi-static tests were performed at a displacement rate of 1 mm/min to capture the AE activity of the samples. Apart from continuous tests, interrupted tests were also performed at specific load intervals, during which through-thickness microscopic inspection was carried out. Test interruptions were performed for every 80 MPa of applied stress from the beginning of the test up to 50 % of the ultimate strength σ_{ult} of each laminate, then every 40 MPa up to 75 % of σ_{ult}, and then finally every 20 MPa till specimen failure. The interrupted tests were controlled in such a way that the damage progression over the total loading regime could be captured, and arranged so that the microscopic inspection rate was increased over time to follow the damage accumulation within the material.
- In a second step, continuous and interrupted load-controlled fatigue tests were performed at a frequency of 3 Hz for a run-out number of cycles equal to one million, at maximum load levels equal to 70 %, 80 % and 90 % of the failure stress σ_{ult}, to correlate the AE activity with the multiaxial stresses.
- Finally, incremental loading tests were performed. During these, the Kaiser effect and the Felicity Ratio (FR) and Calm Ratio (CR) were studied [29-30]. For each loading condition at least three samples from both laminates were tested for statistically acceptable results.

2.3. Acoustic Emission

The elastic waves were captured and transformed into electric signals (AE hits) using a Mistras Group system equipped with the AEwin software. Two Pico piezoelectric sensors (with peak frequency at 450 kHz) were placed on the sample at a relative distance of 80 mm from centre to centre. Vaseline was applied between the sensors and the sample to guarantee the acoustic coupling. An amplitude threshold of 35
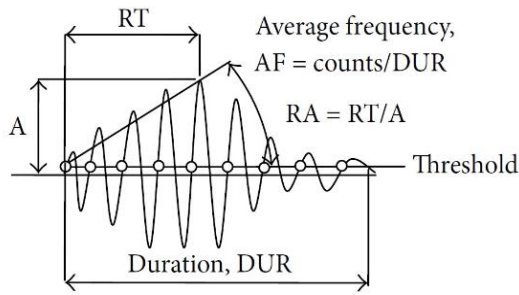
Fig. 2. Typical AE waveform [32].

Fig. 3. Definition of Kaiser and Felicity effects.

dB was applied to filter out mechanical noise, and the signals were amplified with a gain of 40 dB using pre-amplifiers. By using the distance between the two sensors as software input, and the automatic onset time as recorded by the acquisition channels, linear localisation of hits was obtained (AE events). By considering only AE events within the sensor distance, excluding the edges, the database mostly includes damage signals, eliminating as much as possible the influence of any mechanical noise (noise from the grips etc.). By applying a supplementary filter in the analysis, all signals having zero energy were eliminated, because noise signals generally depict low energy content [31]. The sampling rate of the acquisition was 10 MHz. The Peak Definition Time (PDT), Hit Definition Time (HDT) and Hit Lockout Time (HLT) parameters were set to 70, 150 and 700 μs respectively, as used in a similar study in literature [13]. Prior to testing, pencil lead breaks were performed to assess the wave velocity (equal to 5962 m/s and 5479 m/s for the $[0^o/30^o]_{2s}$ and $[0^o/60^o]_{2s}$ lay-ups respectively).

Among the most regularly studied AE features, also investigated in this work, are the absolute energy of the signal, expressed in aJ (10^{-18} J), indicative of the wave intensity, and the Rise Time (RT), expressed in μs, defined as the time from the first threshold crossing of a signal until the time it reaches its maximum amplitude (**Fig. 2**). The Average Frequency (AF), expressed in kHz, is also examined in this analysis. AF is measured in the time domain by the number of threshold crossings over the signal duration and is a representative parameter for the main frequency content of the waveform. After having performed thorough data analysis, it was concluded that the RT and AF were the most sensitive descriptors to identify differences between the two examined angle-ply laminates. A plethora of other descriptors were also evaluated during the AE feature analysis, including the amplitude, the duration and the counts of the recorded waveforms. However, the RT and the AF presented the more pronounced differences when the stress state in the considered composite material was altered. Moreover, during incremental loading the Kaiser and Felicity effects were investigated. The Kaiser effect occurs when AE activity initiates during a loading cycle only at a stress level equal to or higher than the maximum stress of the previous loading cycle (**Fig. 3**). In order to demonstrate the Felicity effect, the FR is defined from the following equation:

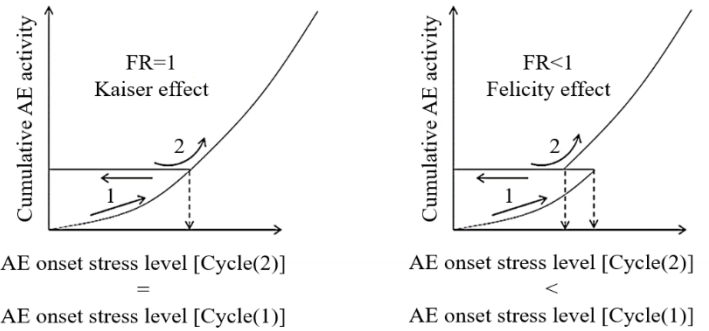$$FR(i+1) = \frac{AE\ onset\ stress\ level\ [Cycle(i+1)]}{Maximum\ stress\ level\ [Cycle\ (i)]} \qquad (1)$$

FR values equal to or higher than unity indicate that negligible or no damage has occurred in the material and that the Kaiser effect takes place. When FR drops below unity, the Kaiser effect does not appear anymore, indicating that damage has been nucleated during the previous loading cycle. In this case the Felicity effect makes its appearance, designating that AE activity initiates earlier than the maximum stress level of the previous cycle (**Fig. 3**). Another parameter that can be used in order to study the structural integrity of the material under incremental loading is the CR, pointing out the AE activity emitted during the unloading stages of the successive cycles. The CR is defined as:

$$CR(i) = \frac{AE\ activity\ (unloading)\ [Cycle(i)]}{AE\ activity\ (loading+unloading)\ [Cycle\ (i)]} \qquad (2)$$

In a sound material CR is close to zero. With the accumulation of damage CR increases, indicating AE activity also during the unloading stages. Exploration of these parameters in composite materials has been performed in the past [29-33] without however targeting quantitative and qualitative correlations with stress or strain states.

2.4. Optical methods

Since AE cannot provide any optical information, two methods were used for damage monitoring and strain measurements. Regarding optical damage monitoring, a Leica MZ125 stereomicroscope with 8-100x magnification range was mounted on the test bench to scan the free edge of the specimen. This allowed damage observations by stopping the test at certain load intervals while still keeping the sample loaded. The damage monitoring during the test interruptions was performed as quickly as possible in order to avoid further damage growth owing to the applied constant load, which was
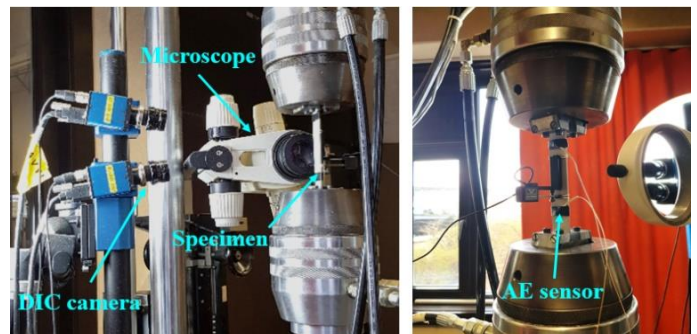

Fig. 4. Experimental set-up.

confirmed by the AE analysis since no acoustic events were located during these interruptions. In order to obtain strain measurements a DIC system, VIC-3D by Correlated Solutions, was utilised. By applying a black/white speckle pattern on the surface of the specimens and by triangulation of two 5 MP Stingray cameras with 23 mm focal length lenses, full field strain maps were obtained. The experimental set-up is presented in **Fig. 4**.

3. Results and discussion

3.1. AE findings during quasi-static loading

The first important finding during the quasi-static tests was the potential of AE to differentiate between laminates with dissimilar multiaxial stress states from early loading stages based on analysis of certain signal features, such as the RT and the AF. Since the different multiaxial stress states are expressed through the λ_{12} ratio, in **Fig. 5** the link between the RT values and the λ_{12} ratio is plotted. This is achieved by taking into account the λ_{12} ratios of the $[0^\circ/30^\circ]_{2s}$ and $[0^\circ/60^\circ]_{2s}$ laminates, which are equal to 2.02 and 0.64 respectively, and by calculating that the same ratio equals 0 in the cross-ply $[0^\circ/90^\circ]_{2s}$ laminates and 5.78 in the shear dominated $[\pm45^\circ]_{2s}$ laminates. These values can be calculated by using the classical laminate theory, as explained in Section 2.1., together with a graphical representation in **Fig. 1**. The data points in **Fig. 5** depict the average RT values recorded between 0 % and 50 % of the testing time in each case, together with the corresponding error bars. This way the AE feature comes from a relatively early state before severe damage influences the original λ ratios. The average values of five specimens for each case are shown. A good repeatability is observed among the iterations, allowing even a separation between the considered cases. Specifically, when shear stresses do not develop, RT averages at approximately 70 μs, while gradually and as λ becomes 5.78, RT climbs to 150 μs. It is evident that higher λ ratios corresponding to higher shear stresses lead to higher RT values, allowing estimation of the dominant stress component in the composite lamina from a relatively early point.

Apart from correlations of the AE features with the different multiaxial stress conditions, correlations with the captured strain field throughout the total testing time could be further obtained. Strains in the material coordinate system of a laminate can only be obtained analytically. Nevertheless, in the angle-ply $[0^\circ/\theta]_{2s}$ laminates, a shear coupling exists also in the geometrical axes owing to the anisotropy of the composite material and the unbalanced stacking sequence [27]. This leads to the appearance of shear strains γ_{xy} under the application of any normal extensional force N_{xx}, which can be measured by DIC on the surface of the specimens. In order to exhibit the existing correlation between the AE signal features and the different shear strains owing to changes of the angle θ, the evolution of the RT as a function of the stress and γ_{xy} (shear strain as measured by DIC) is plotted in **Fig. 6** for both the angle-ply laminates and the cross-ply laminates (with the period of the moving average curve corresponding to 5 % of the data points in each case).
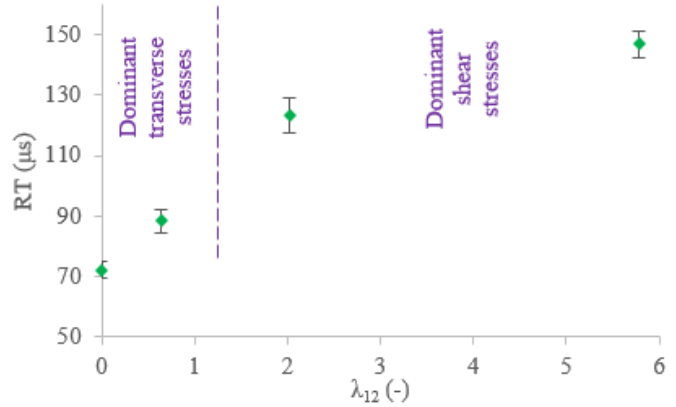

Fig. 5. Dependence of RT on the λ_{12} ratio as obtained from the moving average curves of different lay-ups at a time range equal to 0-50 % of the total testing time.
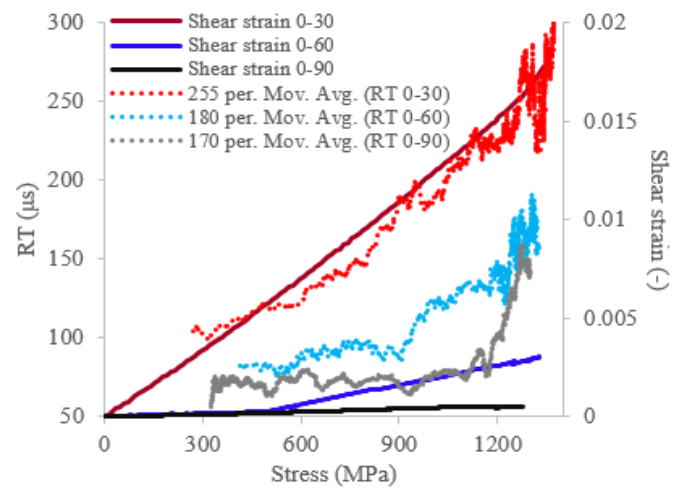

Fig. 6. Evolution of RT versus the stress and the shear strain γ_{xy} of the unbalanced angle-ply and the cross-ply laminates.

It is clear that for the $[0^\circ/30^\circ]_{2s}$ laminates the RT presents a continuously increasing trend from an early stage of the test, following a steady increase of γ_{xy} and the corresponding internal shear damage. The average RT values initiate from around 100 μs and they arise to high values, close to 250 μs, following the appearance of interlaminar delaminations between the laminate layers. These delaminations were the first visible damage incidents microscopically observed in the $[0^\circ/30^\circ]_{2s}$ laminates at around 1000 MPa of the global stress, before any visible matrix cracks in the off-axis plies (**Fig. 7**).

On the other hand, in the $[0^\circ/90^\circ]_{2s}$ laminates, γ_{xy} shows negligible increasing trends, similarly to the RT trendline, which remains at low levels of around 70 μs, before rising at the end due to the occurrence of delaminations. The shear strain of the $[0^\circ/60^\circ]_{2s}$ laminates presents a behaviour in between the two previous cases, being initially low but starting to increase at around 600 MPa, clearly deviating from the $[0^\circ/90^\circ]_{2s}$ case. Interestingly, the same applies for the RT curve which is constantly higher than the one from the $[0^\circ/90^\circ]_{2s}$ laminates, leading again to a sudden increase due to the emergence of delaminations. Matrix cracking was the first damage mode recorded in the $[0^\circ/60^\circ]_{2s}$ laminates from a stress equal to 600 MPa on average (**Fig. 8a**). Interlaminar delaminations occurred late in the test, at a stress greater than

90 % of the ultimate stress (around 1200 MPa), like indicatively shown in **Fig. 8b**.

Thus, it is evident that the AE features can be correlated not only with the different damage modes but also with the dominant stresses/strains in the lamina level even when no visible damage occurs. This sensitivity between the shear strain and the rise time is detected for the first time in polymer composites and opens the potential of AE for prediction of the damage behaviour, as an advancement of the post-damage assessment that has already been investigated in literature.
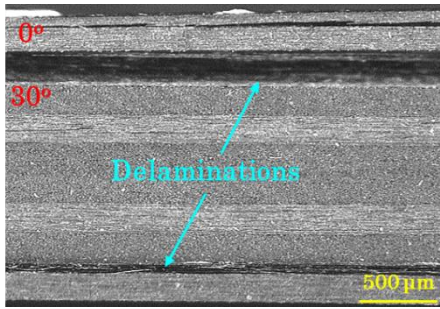

Fig. 7. Damage state in $[0°/30°]_{2s}$ angle-ply laminates at 1100 MPa stress.
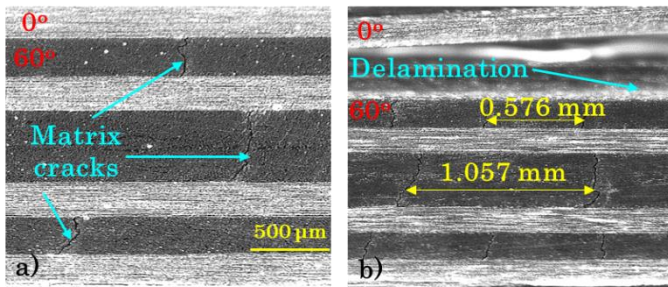
Fig. 8. Damage state in $[0°/60°]_{2s}$ angle-ply laminates at a) 600 MPa and b) 1200 MPa stress.

To obtain a certain quantitative insight into the AF and the AE signal energy content of the angle-ply laminates, **Figs. 9a** and **9b** plot the average AF and absolute energy values at indicative stress stages. Regarding the AF, constantly lower values are registered for the $[0°/30°]_{2s}$ laminates due to the dominant shear stresses. Especially combination of shear damage with delaminations towards final failure leads to very low AF values, close to 50 kHz. When transverse stresses and matrix cracking are dominant, higher AF values are recorded, as shown for the $[0°/60°]_{2s}$ laminates [34]. Regarding the energy values, until 900 MPa the average absolute energy for the $[0°/30°]_{2s}$ case remains quite low, possibly due to the appearance of intralaminar shear debondings only. Beyond this stress, the energy increases due to the emergence of delaminations and fibre breaks. In the $[0°/60°]_{2s}$ laminates higher energy is observed in the 700-1200 MPa stress range due to the occurrence of matrix cracks. After 1200 MPa, an increase in the absolute energy is registered, due to interlaminar delaminations and fibre breaks [35]. These results prove that for the same external stress on the two laminates, significant differences in the AE features are obtained due to the dissimilar stresses in the material coordinate system even prior to the occurrence of microscopically visible damage. It is shown that AE is sensitive not only to the actual damage but also to the stress field that will eventually result in a certain damage mechanism. Moreover, despite the fact that damage at early loading stages is not yet manifested in a form visually observable by the applied monitoring methods, the sensitivity of AE allows detecting phenomena in the scale of aJ.
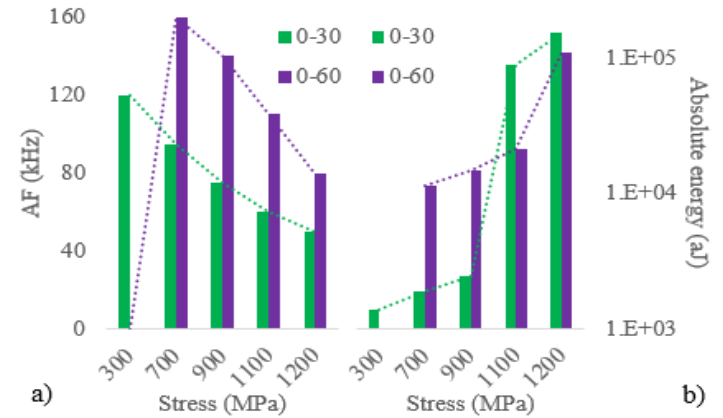

Fig. 9. Evolution of a) AF and b) absolute energy versus the stress of the $[0°/30°]_{2s}$ and $[0°/60°]_{2s}$ laminates.

3.2. AE findings during fatigue loading

The connection between AE and the strain field and damage accumulation is also evident for the specific material in fatigue tests. Initially, the cumulative AE curves are briefly described as shown in **Fig. 10**, plotting the AE activity of two $[0°/30°]_{2s}$ and $[0°/60°]_{2s}$ specimens tested under a maximum stress level equal to 70 % of σ_{ult}. Three stages can be indicatively identified during the evolution of the AE activity, even if not strictly mathematically defined, independently of the applied loading conditions. The first one corresponds to the rapid formation of damage during the very first fatigue cycles, both in the form of intralaminar shear damage, matrix cracks and interlaminar delaminations, as seen for both samples in **Fig. 10**. The second stage continues with a decrease in the slope of the AE activity but with an obvious steady increase of the emitted AE events and can also be identified for both specimens in **Fig. 10**. The last stage appears with a very high increase in the slope of the AE events, signifying the upcoming final failure. This last stage was only present for samples failing before one million cycles (like the $[0°/30°]_{2s}$ specimen reaching only 648595 cycles) and not for those surpassing this run-out value (like the $[0°/60°]_{2s}$ specimen). Despite the fewer fatigue cycles for the shear dominated $[0°/30°]_{2s}$ specimen, significantly more intense AE activity is registered in this case due to the continuous intralaminar shear damage development.

The rise time of the AE signals seemed to be also in the case of fatigue loading the most sensitive descriptor, distinguishing between lay-ups with dominant tensile or shear damage. In **Fig. 11** the RT evolution versus the normalised fatigue life is plotted for the same two $[0°/30°]_{2s}$ and $[0°/60°]_{2s}$ specimens. To display the RT evolution, the moving average of the last 255 data points is shown. An interesting distinction between the two samples can be clearly noticed.
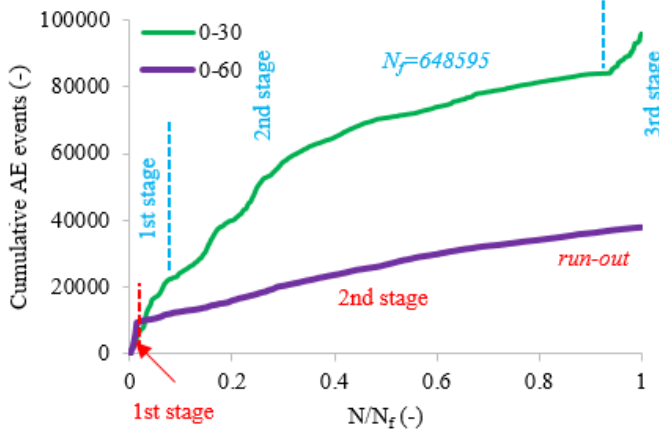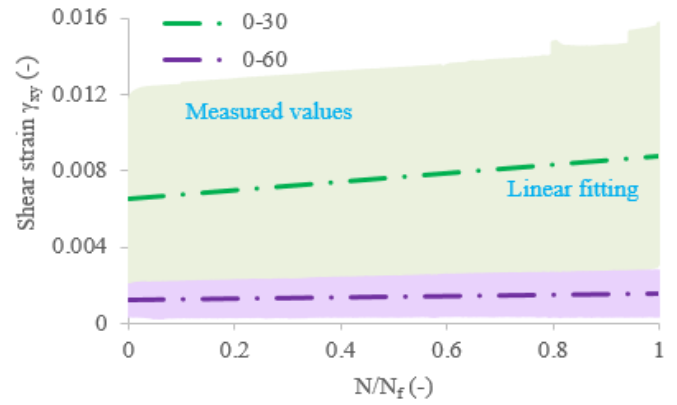
Fig. 10. Evolution of AE activity versus the normalised fatigue life of a $[0°/30°]_{2s}$ and a $[0°/60°]_{2s}$ laminate for the 70 % test.
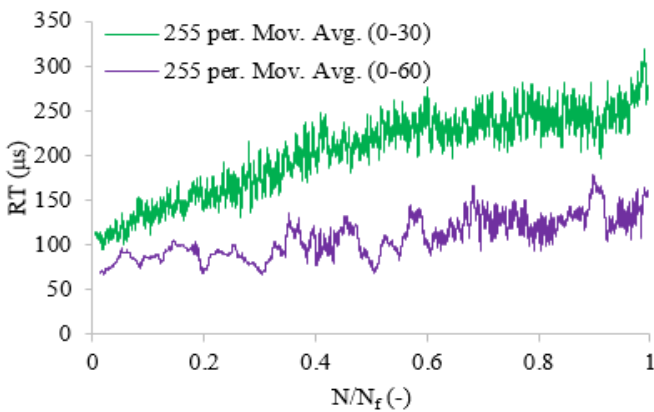
Fig. 11. Evolution of RT versus the normalised fatigue life of a $[0°/30°]_{2s}$ and a $[0°/60°]_{2s}$ laminate for the 70 % test.

Even from the early fatigue cycles, lower RT values are recorded in the $[0°/60°]_{2s}$ sample (**Fig. 11**), corresponding to the development of lower shear stresses and coming to agreement with the trends obtained from the AE analysis of the static tests. A steadily increasing RT evolution is monitored as the fatigue test continues, nicely corresponding to the slow development of delaminations. On the contrary, higher RT values are captured even from the beginning of the fatigue life for the shear dominated $[0°/30°]_{2s}$ sample. The severe accumulation of delaminations is further reflected in the constantly increasing RT values. Furthermore, a characteristic increase in the average RT values is recorded after approximately 90 % of the fatigue life, forewarning about the upcoming catastrophic failure (not evident for the $[0°/60°]_{2s}$ specimen reaching the run-out value of one million fatigue cycles).

In order to confirm the characteristic correlation of the acoustic features not only with the progressive damage spread but with the stress/strain fields as well, **Fig. 12** plots the evolution of the shear strain γ_{xy}, as measured by DIC, versus the normalised fatigue life for both angle-ply laminates. It is obvious that significantly higher shear strains are measured for the $[0°/30°]_{2s}$ sample, which can be identified by the AE analysis, demonstrating higher RT values for this lay-up from the very first fatigue cycles and for the total fatigue life compared to the $[0°/60°]_{2s}$ specimen.


Fig. 12. Evolution of the shear strain γ_{xy} versus the normalised fatigue life of a $[0°/30°]_{2s}$ and a $[0°/60°]_{2s}$ laminate for the 70 % test.

3.3. AE findings during incremental loading

Considering the fact that the failure stress σ_{ult} of the $[0°/30°]_{2s}$ laminates was found to be equal to 1375 MPa, whereas for the $[0°/60°]_{2s}$ laminates it equalled 1318 MPa on average [27,36], incremental tests were finally performed with six successive steps at maximum stress levels of 220, 440, 660, 880, 1100 and 1200 MPa. The last loading step continued until the failure of the specimens.

Starting with the interpretation of the incremental loading response of the examined lay-ups, the difference in the AE activity between the $[0°/30°]_{2s}$ and $[0°/60°]_{2s}$ laminates is indicatively displayed in **Fig. 13** for the 0-1200-0 MPa loading-unloading cycle. It is clear that certain differences arise between the two laminates. Apart from the intensity of the AE activity, which is always higher for the shear dominated $[0°/30°]_{2s}$ laminates, one of the major differences concerns the onset of AE during the consecutive loading cycles or else the appearance of the Kaiser and Felicity effects. In order to demonstrate the different response of the laminates during the incremental loading, **Fig. 14** plots the evolution of the measured Felicity ratio FR versus the maximum stress of each successive loading step. For calculating the FR, the AE onset was assumed to coincide with the appearance of the very first AE event during the loading regime of each cycle. In cases that the Kaiser effect still appeared in the laminates, mainly during the initial loading cycles, the FR was assumed equal to one even if greater values were potentially obtained.
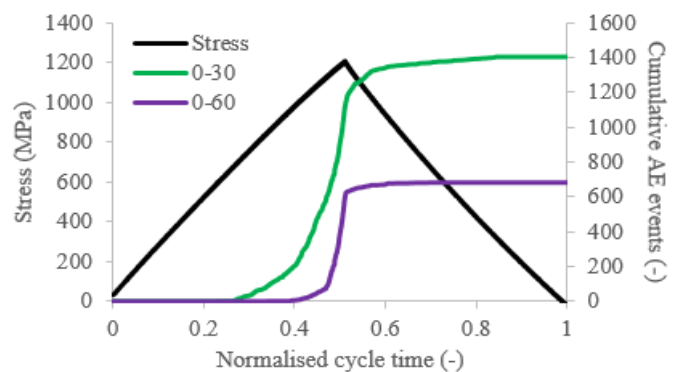
Fig. 13. AE activity versus the stress and the normalised time of the $[0°/\theta°]_{2s}$ lay-ups for the 0-1200-0 MPa loading-unloading cycle.

Looking initially at the 0-440 MPa loading step, the Kaiser effect is evident for both samples. The forming microdamage is of such a small scale that results in FR values equal to one. The first deviation occurs in the 0-660 MPa loading cycle. The Felicity effect has appeared for the $[0°/30°]_{2s}$ specimens with an FR value equal to 0.93, while the $[0°/60°]_{2s}$ laminates are still under the Kaiser effect. Until a stress of 1100 MPa the FR constantly decreases for the $[0°/30°]_{2s}$ laminates, following the increase of shear stresses and the growth of intralaminar debondings. Contrarily, in the $[0°/60°]_{2s}$ specimens the Felicity effect appears during the 4th loading step for the first time. Comparing the FR until 1100 MPa for both laminates, notably lower values can be observed for the $[0°/30°]_{2s}$ laminates. This indicates that the internal shear damage in this lay-up is linked to more brittle behaviour and to fracture surfaces being able to generate AE earlier than the matrix cracks in the $[0°/60°]_{2s}$ samples, having a more elastic response and smoother fracture surfaces. To verify this assumption, in **Fig. 15** post-mortem microscopy images from a section in the middle of the two angle-ply laminates at a stress equal to 400 MPa are shown (obtained after stopping the tests at this stress level and cutting the specimens in the middle). It is obvious that in the $[0°/30°]_{2s}$ laminates matrix-fibre debondings have already occurred, logically attributed to the high shear stresses in the 30° layers, whilst clear surfaces still appear in the $[0°/60°]_{2s}$ laminates with no obvious intralaminar decohesions. In the 0-1200 MPa loading step a notable decrease of the FR occurs for the $[0°/30°]_{2s}$ laminates, which reaches a value equal to 0.63. This corresponds to the formation of delaminations during the previous loading step, showing that the permanent damage caused by the delaminated layers is able to produce early AE activity. This is confirmed in the $[0°/60°]_{2s}$ laminates for which a significant decrease is shown at the last step, corresponding to the growth of delaminations.

Fig. 14. FR evolution versus the maximum stress of succeeding loading-unloading cycles for the $[0°/θ]_{2s}$ laminates.

Fig. 16 plots the calm ratio evolution versus the maximum stress of the consecutive cycles for both CFRP laminates. It is clear that an increasing tendency appears in all cases, related to the continuously developing damage, leading to the release of more and more AE signals when unloading takes place. However, a clear differentiation in the CR values between the two laminates can be observed due to the dissimilar multiaxial stresses, reported for the first time in literature for polymer composites. Even from the early loading cycle at 440 MPa,

higher CR values are recorded for the shear dominated laminates. The shear debondings seem to generate a certain friction not solely when the load increases, but also during the unloading stages. Contrarily, the fracture surfaces developed by the matrix cracks in the laminates with 60° off-axis layers seem to generate less AE activity when the load drops. In all cases, similarly to the FR evolution, sudden changes in the CR value are captured when severe damage occurs in the material, especially in the form of delaminations. Combining FR, CR and feature analyses in composites can thus provide reliable damage evaluations even from primary loading levels.
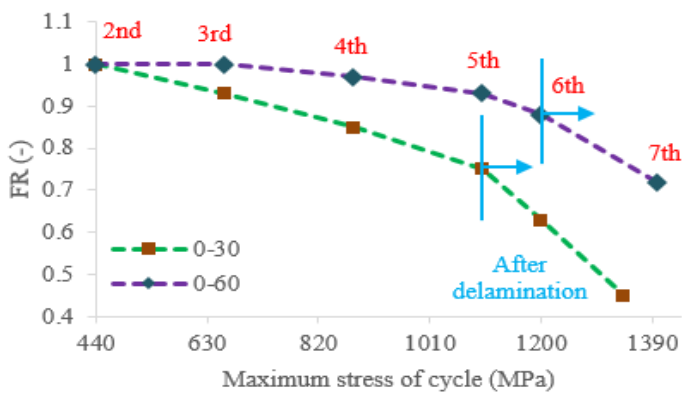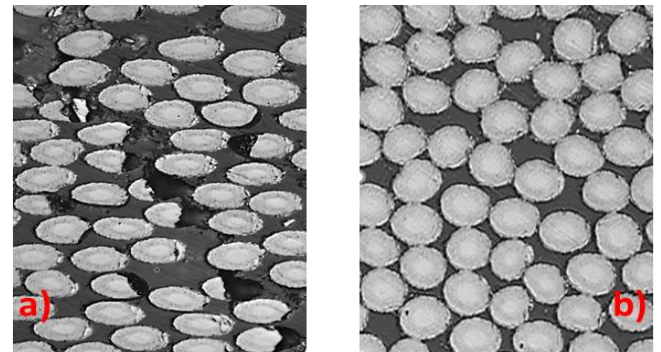

Fig. 15. Post-mortem microscopy images at 400 MPa applied stress for a) $[0°/30°]_{2s}$ and b) $[0°/60°]_{2s}$ laminates.

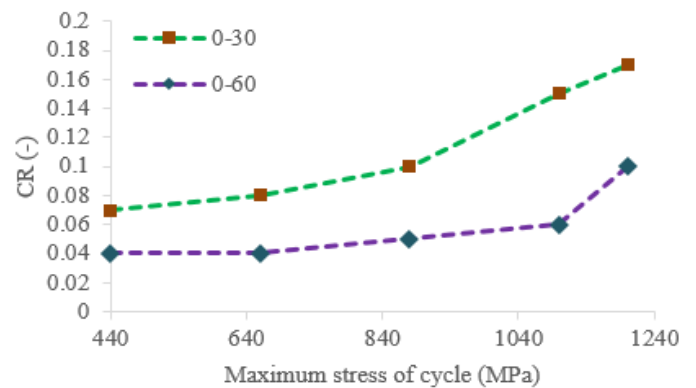**Fig. 16.** CR evolution versus the maximum stress of succeeding loading-unloading cycles for the $[0°/θ]_{2s}$ laminates.

4. Conclusions

Two carbon/epoxy laminates, namely $[0°/30°]_{2s}$ and $[0°/60°]_{2s}$, were tested during this experimental campaign. The laminates, characterised by dominant shear and transverse stresses respectively in their off-axis plies, were examined under quasi-static, fatigue and incremental loading. AE was constantly applied with the aim to examine the potential of the method to indicate the dominant stress/strain component rather than just the appearing damage mode. It was concluded that certain AE features, such as the rise time, the average frequency, the Felicity ratio FR and the calm ratio CR can be used even from early loading stages for the discrimination between laminates with different stress components. This opens the way for acoustic emission to be used for the prediction of the upcoming response of polymer composites rather than just the post-damage assessment that has been mainly investigated so far in literature.

Acknowledgements

References

[1] M. Wevers, Listening to the sound of materials: acoustic emission for the analysis of material behaviour, NDT & E International, 30(2) (1997) 99–106.

[2] Y.H. Yu, J.H. Choi, J.H. Kweon, D.H. Kim, A study on the failure detection of composite materials using an acoustic emission, Composite Structures, 75(1-4) (2006) 163–169.

[3] V. Munoz, B. Vales, M. Perrin, M.L. Pastor, H. Welemane, A. Cantarel, M. Karama, Damage detection in CFRP by coupling acoustic emission and infrared thermography, Composites Part B: Engineering, 85 (2016) 68–75.

[4] M. Giordano, A. Calabro, C. Esposito, A. D'Amore, L. Nicolais, An acoustic-emission characterization of the failure modes in polymer-composite materials, Composites Science and Technology, 58(12) (1998) 1923–1928.

[5] M. Fotouhi, M.A. Najafabadi, Acoustic emission-based study to characterize the initiation of delamination in composite materials, Journal of Thermoplastic Composite Materials, 29(4) (2016) 519–537.

[6] S. Barré, M.L. Benzeggagh, On the use of acoustic emission to investigate damage mechanisms in glass-fibre-reinforced polypropylene, Composites Science and Technology, 52(3) (1994) 369–376.

[7] E.Z. Kordatos, K.G. Dassios, D.G. Aggelis, T.E. Matikas, Rapid evaluation of the fatigue limit in composites using infrared lock-in thermography and acoustic emission, Mechanics Research Communications, 54 (2013) 14–20.

[8] G. Minak, A. Zucchelli, Damage evaluation and residual strength prediction of CFRP laminates by means of acoustic emission techniques, in: L.P. Durand (Ed.), Composite Materials Research Progress, 2008, pp. 165–207.

[9] V. Carvelli, A. D'Ettorre, S.V. Lomov, Acoustic emission and damage mode correlation in textile reinforced PPS composites, Composite Structures, 163 (2017) 399–409.

[10] W. Roundi, A. El Mahi, A. El Gharad, J.L. Rebiere, Acoustic emission monitoring of damage progression in glass/epoxy composites during static and fatigue tensile tests, Applied Acoustics, 132 (2018) 124–134.

[11] D.G. Aggelis, N.M. Barkoula, T.E. Matikas, A.S. Paipetis, Acoustic emission monitoring of degradation of cross ply laminates, The Journal of the Acoustic Society of America, 127(6) (2010) 246–251.

[12] A.J. Brunner, Identification of damage mechanisms in fiber-reinforced polymer-matrix composites with acoustic emission and the challenge of assessing structural integrity and service-life, Construction and Building Materials, 173 (2018) 629–637.

[13] N. Godin, S. Huguet, R. Gaertner, L. Salmon, Clustering of acoustic emission signals collected during tensile tests on unidirectional glass/polyester composite using supervised and unsupervised classifiers, NDT & E International, 37(4) (2004) 253–264.

[14] V. Kostopoulos, T.H. Loutas, A. Kontsos, G. Sotiriadis, Y.Z. Pappas, On the identification of the failure mechanisms in oxide/oxide composites using acoustic emission, NDT & E International, 36(8) (2003) 571–580.

[15] Y. Mizutani, K. Nagashima, M. Takemoto, K. Ono, Fracture mechanism characterization of cross-ply carbon-fiber composites using acoustic emission analysis, NDT & E International, 33(2) (2000) 101–110.

[16] J. Martínez-Jequier, A. Gallego, E. Suárez, F.J. Juanes, Á. Valea, Real-time damage mechanisms assessment in CFRP samples via acoustic emission Lamb wave modal analysis, Composites Part B: Engineering, 68 (2015) 317–326.

[17] F.E. Oz, N. Ersoy, S.V. Lomov, Do high frequency acoustic emission events always represent fibre failure in CFRP laminates?, Composites Part A: Applied Science and Manufacturing, 103 (2017) 230–235.

[18] F.E. Oz, N. Ersoy, M. Mehdikhani, S.V. Lomov, Multi-instrument in-situ damage monitoring in quasi-isotropic CFRP laminates under tension, Composite Structures, 196 (2018) 163–180.

[19] M.G. Stout, D.A. Koss, C. Liu, J. Idasetima, Damage development in carbon/epoxy laminates under quasi-static and dynamic loading, Composites Science and Technology, 59(16) (1999) 2339–2350.

[20] M. Quaresimin, 50th anniversary article: multiaxial fatigue testing of composites: from the pioneers to future directions, Strain, 51(1) (2015) 16–29.

[21] H. Pakdel, B. Mohammadi, Experimental observation and energy based analytical investigation of matrix cracking distribution pattern in angle-ply laminates, Theoretical and Applied Fracture Mechanics, 92 (2017) 146–154.

[22] M.G.R. Sause, T. Müller, A. Horoschenkoff, S. Horn, Quantification of failure mechanisms in mode-I loading of fiber reinforced plastics utilizing acoustic emission analysis, Composites Science and Technology, 72(2) (2012) 167–174.

[23] M. R'Mili, M. Moevus, N. Godin, Statistical fracture of E-glass fibres using a bundle tensile test and acoustic emission monitoring, Composites Science and Technology, 68(7-8) (2008) 1800–1808.

[24] M. Saeedifar, D. Zarouchas, Damage characterization of laminated composites using acoustic emission: A review, Composites Part B: Engineering, 195 (2020) 108039.

[25] C. Barile, C. Casavola, G. Pappalettera, V.P. Kannan, Application of different acoustic emission descriptors in damage assessment of fiber reinforced plastics: A comprehensive review, Engineering Fracture Mechanics, 235 (2020) 107083.

[26] M. Sause, M. Hamstad, 7.14 Acoustic Emission Analysis, in: P.W.R. Beaumont, C.H. Zweben (Eds.), Comprehensive Composite Materials II, Oxford: Academic Press, 2018, vol. 7, pp. 291–326.

[27] K.A. Kalteremidou, M. Hajikazemi, W. Van Paepegem, D. Van Hemelrijck, L. Pyl, Effect of multiaxiality, stacking sequence and number of off-axis layers on the mechanical response and damage sequence of carbon/epoxy composite laminates under static loading, Composites Science and Technology, 190 (2020) 108044.

[28] ASTM D3039, Standard test method for tensile properties of polymer matrix composite materials (2008).

[29] K. Ono, A. Gallego, Research and applications of AE on advanced composites, Journal of Acoustic Emission, 30 (2012) 180–229.

[30] J.M. Waller, E. Andrade, R.L. Saulsberry, Use of acoustic emission to monitor progressive damage accumulation in Kevlar® 49 composites, in: AIP Conference Proceedings, American Institute of Physics, 1211(1) (2010) 1111–1118.

[31] T.P. Philippidis, V.N. Nikolaidis, J.G. Kolaxis, Unsupervised pattern recognition techniques for the prediction of composite failure, Journal of Acoustic Emission, 17(1) (1999) 69–81.

[32] D.G. Aggelis, K.G. Dassios, E.Z. Kordatos, T.E. Matikas, Damage accumulation in cyclically-loaded glass-ceramic matrix composites monitored by acoustic emission, The Scientific World Journal, 2013 (2013) 869467.

[33] S. Esola, B. Wisner, P. Vanniamparambil, J. Geriguis, A. Kontsos, Part qualification methodology for composite aircraft components using acoustic emission monitoring, Applied Sciences, 8 (2018) 9:1490.

[34] L. Li, S.V. Lomov, X. Yan, V. Carvelli, Cluster analysis of acoustic emission signals for 2D and 3D woven glass/epoxy composites, Composite Structures, 116 (2014) 286–299.

[35] N. Chandarana, D.M. Sanchez, C. Soutis, M. Gresil, Early damage detection in composites during fabrication and mechanical testing, Materials, 10(7) (2017) 685.

[36] K.A. Kalteremidou, B.R. Murray, E. Tsangouri, D.G. Aggelis, D. Van Hemelrijck, L. Pyl, Multiaxial damage characterization of carbon/epoxy angle-ply laminates under static tension by combining in situ microscopy with acoustic emission, Applied Sciences, 8(11) (2018) 2021.